Journal of Radiation and Nuclear Applications
An International Journal

http://dx.doi.org/10.18576/jrna/090309

Synthesis, Structure, and Gamma-Ray Shielding Properties of Phosphate Glass Doped with Naturally Extracted Neodymium

M. S. Hafiz [1*], *M. G. El-Feky* [1], *Eman Ibrahim* [1], *N.S. Gomaa* [2], *Atef El-Taher* [3].

[1]Geochemical Exploration Department, Nuclear Materials Authority (NMA), P.O. Box 530, El-Maadi, Cairo, Egypt.
[2]Physics Department, Faculty of Science Al-Azhar University, Nasr City,11884, Cairo, Egypt.
[3]Physics Department, Al-Azhar University, Faculty of Science, Assuit 71452, Egypt.

Received: 2 Jun. 2024, Revised: 22 Jul. 2024, Accepted: 1 Aug. 2024.

Published online: 1 Sep 2024

Abstract: Herein, an efficient new glass series was prepared via the melt-quenching method, with the composition (62-x)$NH_4H_2PO_4$ + 20B_2O_3 + 5ZnO + 10Bi_2O_3 + 3Na_2CO_3 + xNd_2O_3, where x takes on the values of 0, 1, 2, and 3 mol%. The glass structure was analyzed using FTIR spectroscopy, density (ρ), molar volume (Mv), and XRD techniques. The glass samples were irradiated with collimated gamma rays at three energy lines of 662, 1173, and 1332 KeV emitted by ^{137}Cs and ^{60}Co, respectively. Radiation shielding parameters such as N_{el} (electron density), Z_{eff} (effective atomic number), HVL (half-value layer), μ/ρ (mass attenuation coefficients), TVL (Tenth value layer), and MFP (mean free path) were theoretically calculated using the XCOM program and experimentally measured with a NaI(Tl) scintillation detector. The theoretical and experimental values of the mass attenuation coefficients exhibit a slight discrepancy (by < 15%). The shielding features are associated with the composition of the investigated phosphate glass samples. Notably, an increase in shielding properties was observed with the increasing Nd_2O_3 content in the structure of the phosphate glass samples.

Keywords: Phosphate glass, Shielding γ-ray, NaI (TL) detector.

1 Introduction

Due to the hazardous gamma radiation (γ-ray) emitted by radioactive sources such as nuclear reactors, nuclear weapons, and nuclear fuel, it is essential to handle and shield these materials appropriately. Without proper shielding, this powerful and penetrating radiation poses a significant threat to plant and animal life, as well as human health. Prolonged exposure to γ-ray can lead to serious health issues, including cancer, tissue damage, and neurological impairments. The effects of such exposure are often irreversible and may even be passed on to future generations. Traditionally, radiation shielding materials have included bricks, concrete, lead, and lead-based alloys.

However, these conventional materials have several practical drawbacks, including significant weight, potential hazards associated with lead, and high opacity.

Recently, researchers in the fields of radiation detection and shielding have explored glass materials that incorporate high Z (atomic weight) elements, like rare earth elements, which offer a more environmentally friendly alternative [1-4]. In light of this interest, researchers are focused on developing a variety of shielding materials, including steel rocks [5], alloys [6-9], slag [10], ferrites [11], polymers [12], nanocomposites [13-15], and glasses [16-21]. Glass-based shielding materials offer advantages such as transparency, reduced weight, and ease of transport. Over time, traditional shielding materials like lead, concrete, and bricks may develop physical fissures or cracks, rendering them less effective for radiation protection and detection applications. In contrast, the amorphous and supercooled liquid nature of glass has led to its investigation for various applications in fields such as medicine, diagnostics, astronomy, optics, and radiation shielding [22-23].

Moreover, glasses possess well-known properties, including lightweight construction, transparency, recyclability, mechanical toughness, chemical inertness, and the ability to be molded into various shapes and sizes [24-26]. Reza Bagheri et al. [24-26] investigated the radiation characteristics of heavy metal oxides, including Bi_2O_3 PbO and BaO. This study employed both experimental measurements and WinXcom software for analysis.

*Corresponding author e-mail: maisaeed366@gmail.com

2 Experiment

2.1 Materials and methods

Natural Nd was utilized in this study, which was extracted as follows: Pure Nd and Nd were separated from a rare earth element (REE) concentrate, prepared from Abu-Zeinema gibbsite ore, using the cation exchange resin Dowex 50W-X8 with a 150 mesh size. Two columns were employed for this separation process: First column, the resin was packed in its hydrogen form and used to create a saturated REE bed. The second one, referred to as the retention column, contained resin that was converted to its Cu(II) form, with a volume twice that of the first column.

REEs were eluted from the first column through the second column using a 0.015 M EDTA solution (in its NH_4^+ form) at a pH=8.5 and a flow rate (1.0 mL/min), corresponding to a 20 min interaction time. The resulting eluate fractions were successfully collected for each distinct pure metal, including Nd, based on variations in the stability constants between EDTA and the individual separated REEs [30].

Other chemicals were high-purity reagents (purity > 99.9%) and were sourced from Prolabo. Four glass samples doped with Nd^{3+} were synthesized using the melt quenching technique, with the following composition: (62-x)NH4H2PO4 +20B2O3 + 5ZnO + 10Bi2O3 + 3Na2CO3 + xNd2O3 [22]. These glass samples are coded as M0, M1, M2, and M3, corresponding to the Nd2O3 content with x = 0, 1.0, 2.0, and 3.0 mol%, respectively, as presented in Table 1. The chemical reagents were mixed thoroughly using a pestle and mortar for over half an hour to prepare 20 ±0.0001 g batches, using an electronic balance (Shimadzu ELB300, Japan). The powdered material was then transferred to a 40 mL porcelain crucible and placed at room temperature in a muffle furnace. The furnace temperature was gradually increased to 1200 °C.

Continuous stirring was performed to prevent the formation of bubbles in the molten material. The melt was then poured into a preheated stainless steel mold and annealed at 350 °C for one hour to minimize thermal stress. The resulting glass samples were polished to achieve optimal flatness with varying thicknesses and were shaped into circular specimens.

2.2 Characterization

X-ray diffraction (XRD). Crystallinity of the glass samples was performed using a Philips PW 3710/31 diffractometer (Philips, Eindhoven, Netherlands), to confirm their amorphous nature. The measurements were conducted at room temperature using CuKα radiation (λ: 1.54 Å) over a 2θ range of 4-80°.

Fourier transform infrared spectroscopy (FTIR). The spectra of the glass samples were collected over the wavenumber range (4000–400 cm^{-1}) using an FTIR spectrophotometer Nicolet 10 (Thermo-Fisher Scientific Inc., MA, USA).

Molar volume and density determination. Density measurements were conducted to characterize the effect of doping Nd_2O_3 on glass structure. The densities of the samples were determined using the Archimedean method (Eq. 1) [31], and the molar volumes were calculated (Eq. 2) [32], as outlined below:

$$\rho_{sample} = \frac{\rho_{liquid} \times m_{air}}{m_{air} - m_{liquid}} \quad (1)$$

$$VM = \frac{M_T}{\rho} \quad (2)$$

where m_{liquid} and m_{air}, represent the sample's weight in immersion toluene and air, respectively, and ρ_{liquid} denotes the toluene's density. The density measurements (ρ) have an accuracy of ±0.001 g/cm³. The total molecular weight is denoted as M_T.

2.3 γ-ray shielding analysis

The narrow beam transmission technique (NBTT) utilizes a well-calibrated 3" x 3" NaI(Tl) scintillation detector, functioning as a γ-ray spectrometer. The detector is protected from induced X-rays using a lead cover (5 cm thick), a lead brick chamber for environmental isolation, and a 0.6 cm thick cylindrical Cu shield. The detector is connected to a Nuclear Enterprises primary shaping amplifier and a Tennelec high-voltage power supply with an HV-digital display. It is linked to a Nuclease PCA-8000 8192 multichannel analyzer, which is computer-based and equipped with a color graphical display and sophisticated technical features. The lead collimator, mounted on the detector cap, was filled with cylindrical pellet samples.

The radiation source was positioned above a hole that aligned with the center of the sample, ensuring that the collimated beam traversed the sample layer before reaching the detector. Fig. 1 illustrates the NBTT used to analyze γ-ray characteristics. Measurements were conducted for half an hour with this setup, focusing on the transmitted I photon and a narrow beam of monoenergetic photons with intensity Io, without the sample pellet.

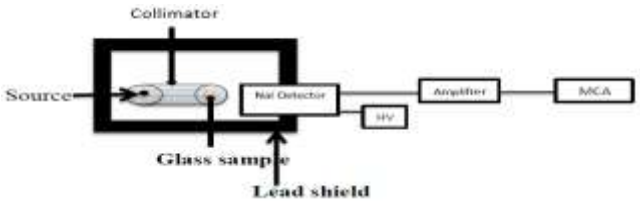

Fig. 1: Geometry of narrow beam transmission technique.

3 Theoretical theory

The shielding characteristics of glass samples against γ-radiation can be determined by calculating shielding parameters such as the mass attenuation coefficient, mean free path and half-value layer.

3.1 Linear attenuation coefficient (μ)

To calculate the shielding parameters, it is essential to determine the μ in cm^{-1}. It was calculated via the Beer-Lambert law, as follows:

$$\mu = \frac{\mathrm{Ln}(\frac{Io}{I})}{x} \qquad (3)$$

where, "*I"* and "*I*o" denote the photon energy counts with and without shielding material thickness, respectively, while "x" represents the material thickness [34].

3.2 Mass attenuation coefficient (μ_m)

This coefficient is primarily influenced by the density of the material used (ρ). Unlike the previous coefficient, it is divided by the material's density, resulting in the mass attenuation coefficient, denoted as 'μm' (cm^2/g) and can be calculated as follows:

$$\mu_m = \mathrm{Ln}\ (I\_o/I)/\rho x \qquad (4)$$

Where ρ represents the shielding material's density [34]. It can be calculated theoretically using NIST XCOM software or practically using any kind of γ-ray detector [35], using relation (5).

$$\mu_m = \sum_i w_i\ \mu_i \qquad (5)$$

Where μ_i and w_i are the proportion of the i^{th} element and the μ_m are used to determine the proportion in the mixed sample.

3.3 Tenth value layer (TVL), half value layer (HVL), and mean free path (MFP)

TVL shielding parameter denotes the thickness of the shielding material needed to diminish gamma energy to a tenth (10%) of its initial intensity, as indicated in Eq. (5). Similarly, the HVL parameter, is defined as the thickness of the shielding material necessary to reduce the intensity of an incident γ-beam to half of its original intensity (Eq. 6) [36, 37].:

Both HVL and TVL parameters are dependent on radiation energy and describe how well γ-energies penetrate the fabricated polymer nanocomposite. Thus, they are crucial for quickly indicating the appropriate shielding properties in distance units (mm/cm) [36, 37].

Finally, the MFP parameter represents the average distance gamma-energies travel through shielding material before being absorbed or scattered (cm). It is mathematically calculated by inverting the μ (Eq. 8) [36, 37]:

$$\mathrm{TVL} = \ln 10/\mu \qquad (5)$$

$$\mathrm{HVL} = \ln 2/\mu \qquad (6)$$

$$\mathrm{MFP} = 1/\mu \qquad (7)$$

Furthermore, the MFP, TVL, and HVL parameters are interconnected as expressed in Eq. (8) [36, 37]:

$$\mathrm{MFP} = \mathrm{HVL}/\ln 2 = \mathrm{TVL}/\ln 10 \qquad (8)$$

3.4 Effective atomic number (Z_{eff}) and electronic density (N_{el})

The Nel, defined as the number of electrons per mass unit, can be calculated using Eq. (9), while the Zeff, equivalent to the atomic number of elements, is another key property crucial for understanding the radiation shielding effectiveness of a compound or mixture [18]:

$$Z_{eff} = \sigma_{(t,a)}/\sigma_{(t,el)} = (\sum_{ini}\ A_i(\mu/\rho)_i)/(\sum_{ini}\ A_i/Z_i(\mu/\rho)_i\ ) \qquad (9)$$

$$N_{el} = \mu_m/\sigma_e = (Z_{eff}\ N_A \sum\_{ini}\ )/M \qquad (10)$$

3.5 Win-XCom program

Using the Win-XCom computer program, the μ_m values for the current glass system were calculated. This software offers total attenuation cross-sections, total mass attenuation coefficients, and partial cross-sections (including photoelectric absorption, coherent and incoherent scattering, and pair formation) for various elements across a photon energy range of 1 keV to 100 GeV [38].

4 Results and Discussion

4.1 Characterization of the glasses

The glass series' XRD pattern is presented in Fig. 2. Notably, no distinct peaks are observable, indicating a lack of crystalline structure. Instead, a prominent hump in the diffraction pattern confirms that the glass samples are amorphous, a typical characteristic of non-crystalline materials where atomic disarray inhibits the formation of sharp diffraction peaks.

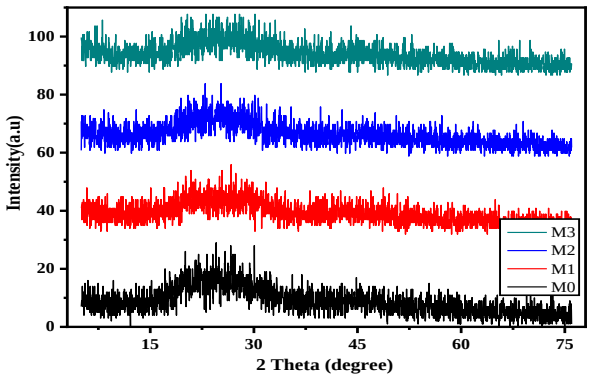

Fig. 2: X-ray diffraction pattern for glass series.

3.2 Density and molar volume measurements

Both density (ρ) and molar volume (VM) are essential parameters for evaluating the physical properties of materials. Table 1 displays the glass samples alongside their respective molar volume and density values. The density of glass increases as Nd_2O_3 is added, correlating with its concentration in the composition. This can be attributed to the fact that doped Nd_2O_3 has a higher molecular weight and density (336.48 g/mole) compared to phosphate oxide (115.03 g/mole) and boron oxide (69.62 g/mole). In the VM measurements, sample M_0 exhibited a decrease to 55.5 cm^3/mol, while sample M_3 showed an increase to 60.8478 cm^3/mol. The produced glass's density and molar volume exhibited an inverse relationship, likely due to structural changes within the glass. The observed decrease in VM values can be attributed to the compaction of the structure, resulting from a reduction in bond length or interatomic spacing among the atoms in the glass network [35].

4.3 FTIR characterization

FTIR analysis is a significant examination that offers a detailed picture and insights into the structural composition of a given system. FTIR posits an independent relationship between the vibrations of structural units and their interaction with the surrounding glass network [36]. Fig. 3 presents the FTIR spectra of various synthesized neodymium-phosphate glasses, along with the corresponding vibrational assignments. Additionally, bands in the 505–525 cm^{-1} region are typically associated with O-P-O bending vibrations. This region may also encompass three vibrations of PO_4^{3-} polyhedra, bending vibrations, and deformation modes of (P–O band) of PO_4^{3-} groups [36].

Other glass networks exhibited Zn–O–Zn vibrations with angular deformations within the range of 560–584 cm^{-1}. The band observed between 629–677 cm^{-1} corresponds to the Bi—O vibrations in [BiO_3] units and the symmetric stretching vibrations of the P—O—P bonds. Additionally, Zn–O–Zn vibrations were detected in the range of 741–748 cm^{-1} [36]. Conversely, these bands were associated with the symmetric P–O–P vibrations. The region between 812 cm^{-1} and 825 cm^{-1} was divided into three distinct modes, which included stretching B–O vibrations of BO_4 units, as well as the stretching and asymmetric stretching modes of P–O–P. The structural units corresponding to the band at 945 cm^{-1} were found to disappear with the ZnO addition. The vibrations of P–O groups, attributed to non-bridging oxygens (NBO), were observed in the band ranging from 1009 to 1030 cm^{-1} [37].

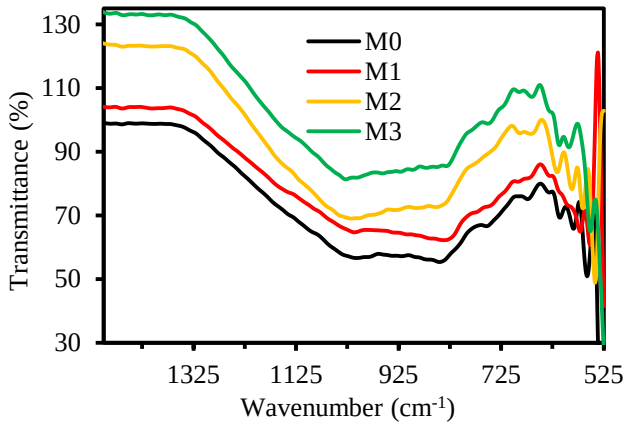

Fig. 3: FTIR spectra of the prepared glass series.

Table 1. Chemical composition, density, and molar volume of manufactured glass samples.

Sample Code	Composition (mol%)						Density (g/cm^3)	Molar volume (cm^3/mol)
	P_2O_5	B_2O_3	ZnO	Bi_2O_3	Na_2CO_3	Nd_2O_3		
M0	62	20	5	10	3	0	3.1384	60.8478
M1	61	20	5	10	3	1	3.2619	59.0054
M2	60	20	5	10	3	2	3.4748	55.8203
M3	59	20	5	10	3	3	3.4940	55.5000

5 Radiation Shielding Parameters Measurements

5.1 The linear attenuation coefficient

The NBTM utilized γ-energies of 0.662, 1.173, and 1.332 MeV, emitted from point sources of ^{137}Cs and ^{60}Co, to evaluate the shielding properties of the produced glass. The thickness (x) of the produced glass samples was precisely determined using a micrometer with ±0.01 mm. The intensity of the emitted and transmitted γ-rays (*Io* and *I*) was experimentally detected using a NaI detector [36]. Table 2 presents the measured μ values.

Table 2. The linear attenuation coefficients (μ, in cm^{-1}) at the selected energies.

Sample code	μ (cm^{-1})		
	0.662 MeV	1.173 MeV	1.332 MeV
M0	0.25	0.18	0.17
M1	0.27	0.19	0.18
M2	0.29	0.21	0.19
M3	0.31	0.23	0.21

The primary interaction in the energy lines examined at 0.662, 1.173, and 1.332 MeV is Compton scattering (CS), as indicated by the observed linear increase. The CS cross-section is directly proportional to the atomic number ($\sigma CS \propto Z$). When Nd_2O_3 was substituted for P_2O_5, the μ values increased from 0.25 to 0.31 cm^{-1} at 0.662 MeV and from 0.17 to 0.21 cm^{-1} at 1.332 MeV as the Nd_2O_3 concentration rose from 0% to 3 mol%. This increase in μ values can be attributed to the higher density and molecular weight of Nd_2O_3 (336.48 g/mol) compared to P_2O_5 (115.03 g/mol). Additionally, as the gamma-photon energy increased, μ values exhibited a linear decrease. This reduction is consistent with the CS cross-section, which is inversely related to gamma-photon energy ($\sigma CS \propto E^{-1}$). In this study, μ values for the M0 glass sample decreased from 0.25 to 0.17 cm^{-1}, while for sample M3, they dropped from 0.31 to 0.21 cm^{-1}, when gamma photon energy was varied between 0.662 and 1.332 MeV.

5.2 The Mass attenuation coefficient

Fig. 4 illustrates the relationship between energy and the mass attenuation coefficient. As the energy changes from 0.662 MeV to 1.332 MeV, the μ_m decreases, indicating greater γ-ray transmission and absorption, along with reduced interaction between the glass samples and the γ-rays. The interactions between γ-rays and the glass samples are characterized by varying energy levels, exhibiting different dominance patterns: pair production occurs at energies above 1.022 MeV, the photoelectric effect is significant at lower energy levels, and Compton scattering is predominant in the intermediate range.

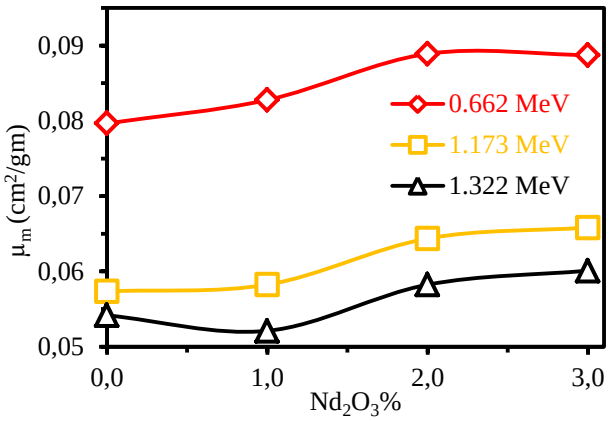

Fig. 4: Variation of μm with Nd2O3 content for glass series at different energies.

Fig.5 shows how the mass attenuation coefficient correlates with neodymium oxide content in the glass system. It demonstrates that the mass attenuation coefficient increases with higher Nd_2O_3 content across all energy levels. This behavior mirrors that of the linear attenuation coefficient, reflecting the greater density and atomic number of neodymium oxide. For instance, the mass attenuation coefficient rises from 0.079658 cm^2/g for sample M0 to 0.089 cm^2/g for sample M3 at 0.662 MeV. This suggests that the glass composition containing 3 mol% neodymium oxide—specifically ($59NH_4H_2PO_4$ + $20B_2O_3$ + 5ZnO + $10Bi_2O_3$ + $3Na_2CO_3$ + $3Nd_2O_3$)—exhibits a higher mass attenuation coefficient due to its increased neodymium oxide concentration. A higher ratio of Nd_2O_3 typically leads to improved mass attenuation in phosphate glass systems.

The mass attenuation coefficients (μ_m) for different composites, elements, and/or elemental mixtures ($Z \leq 100$) within the photon-energy range of 1 keV to 100 GeV were theoretically calculated using the XCOM program. This theoretical framework allowed for the validation of the accuracy of the experimentally determined mass attenuation coefficients. The calculation of mass attenuation is performed using Eq. (5) [39]. Table 3 presents a comparison of the theoretical and experimental μ/ρ values. The deviation (Dev%) between these two methods can be calculated using the following formula:

$$\text{Dev } \% = \frac{\mu_{m\,(th)} - \mu_{m\,(exp)}}{\mu_{m\,(th)}} \times 100 \qquad (11)$$

The observed deviation was found to be less than 10%, suggesting a minimal discrepancy between the predicted and measured mass attenuation coefficients for the synthesized phosphate glass doped with neodymium oxide across different energy levels [40]. This variation can be attributed to differences in the applied technique databases and the extended nuclear cross-section libraries used [41].

Glass sample M3 exhibited the highest mass attenuation coefficient of 0.089 cm²/g. When compared to the value for lead (0.1101 cm²/g), this represents 81% of the shielding effectiveness of lead [42, 43]. These findings confirm that neodymium oxide-doped phosphate glass is a highly effective material for gamma radiation shielding.

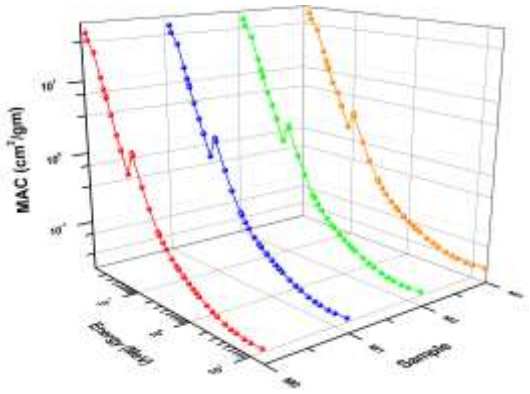

Fig.5: The estimated μm values about photon energy in the energy range 0.015-15 MeV.

5.3 The Half value layer, tenth value layer and Mean Free Path

The choice of shielding material for application is influenced by the Half Value Layer (HVL) shielding parameter, which is defined as the thickness of the shielding material that, according to equation 6, reduces the initial intensity of gamma rays to its half value. The tenth layer of value: This shielding parameter, which is the same as HVL, may be calculated using equation 7 and represents the thickness of the shielding material that reduces gamma ray intensity to a tenth of its initial intensity. [44, 45].

The HVL, TVL, and MFP should be as low as feasible. The values that were obtained are tabulated in Table 4. The relationship between HVL, TVL, and mfp with energy (MeV) is shown in Figures 6, 7, and 8, respectively. These figures demonstrate how adding Nd2O3 significantly reduces mfp, TVL, and HVL. This is because Nd_2O_3 has a high atomic number and density, which causes the densities of the glass samples to rise. At 0.662 MeV, HVL decreased for glass samples from the glass series from 2.77, 3.85, and 4.07 to 2.23, 3.01, and 3.3. MFP and TVL exhibit the same characteristics as HVL. The M3 glass sample, which is composed of ($59\%NH4H_2\ PO_4$ $+20\%B_2O_3$ $+5\%ZnO$ $+10\%Bi_2O_3$ $+3\%Na_2CO_3$ $+3\%Nd_2O_3$), is the best [46].

Table 3: Mass attenuation coefficients, both theoretical and experimental, for the glass samples at various energies and the associated deviation.

Energy	0.662 MeV			1.173 MeV			1.332 MeV		
Sample	HVL	TVL	MFP	HVL	TVL	MFP	HVL	TVL	MFP
M0	2.77	9.21	4	3.85	12.7	5.555	4.07	13.5	5.88
M1	2.56	8.52	3.703	3.648	12.1	5.263	4	13	5.8
M2	2.39	7.93	3.571	3.465	10.9	5	3.64	12.1	5.2
M3	2.23	7.42	3.448	3.15	10	4.545	3.3	10.9	4.74

Table 4: HVL, TVL, and MFP (in cm) values for prepared glass samples at various energies.

Energy (MeV)	0.662		1.173		1.332	
Sample	μ_m (ex)	μ_m (th)	μ_m (ex)	μ_m (th)	μ_m (ex)	μ_m (th)
M0	0.079 ±0.006	0.07	0.057 ±0.003	0.05	0.05 ±0.002	0.054
M1	0.082 ±0.005	0.07	0.058 ±0.003	0.05	0.05 ±0.004	0.054
M2	0.088 ±0.01	0.07	0.064 ±0.010	0.05	0.05 ±0.007	0.054
M3	0.088 ±0.011	0.07	0.065 ±0.013	0.05	0.06 ±0.010	0.054

N.B.: ex: The theoretical μm and μth: the experimental μm.

5.3 The Half value layer, tenth value layer and Mean Free Path

The choice of shielding material for application is influenced by the Half Value Layer (HVL) shielding parameter, which is defined as the thickness of the shielding material that, according to equation 6, reduces the initial intensity of gamma rays to its half value. The tenth layer of value: This shielding parameter, which is the same as HVL, may be calculated using equation 7 and represents the thickness of the shielding material that reduces gamma ray intensity to a tenth of its initial intensity. [44, 45].

The HVL, TVL, and MFP should be as low as feasible. The values that were obtained are tabulated in Table 4.

The relationship between HVL, TVL, and mfp with energy (MeV) is shown in Figures 6, 7, and 8, respectively. These figures demonstrate how adding Nd2O3 significantly reduces mfp, TVL, and HVL. This is because Nd_2O_3 has a high atomic number and density, which causes the densities of the glass samples to rise. At 0.662 MeV, HVL decreased for glass samples from the glass series from 2.77, 3.85, and 4.07 to 2.23, 3.01, and 3.3. MFP and TVL exhibit the same characteristics as HVL. The M3 glass sample, which is composed of (59%$NH4H_2$ PO_4 +20%B_2O_3 +5%ZnO +10%Bi_2O_3 +3%Na_2CO_3 +3%Nd_2O_3), is the best [46].

5.4 γ-ray attenuation features within the energy range (0.015 to 15 MeV)

Furthermore, to comprehensively understand how photon energy affects the variance in μ/ρ values for the current samples, the μ/ρ values of the produced glasses were assessed using WinXcom software across an energy range of 0.015 to 15 MeV. Fig. 5 displays the μ/ρ analysis results within the 0.015 to 15 MeV range, as a function of photon energy, showing that μ/ρ values in the glass sample fluctuate with changes in incident photon energy and Nd content. The μ/ρ values increase with higher neodymium concentration and decrease with increasing photon energy, exhibiting a notable peak at 98 keV, attributable to the K X-ray absorption edge for bismuth (Bi) metal. The variation in μ/ρ values with photon energy can be explained by partial radiation interaction processes, including pair production (PP), Compton scattering (CS), and photoelectric effect (PE). The pair production (PP) action mechanism results in a gradual increase in μ/ρ values within the high-energy range of 1.022 to 15.0 MeV. In the intermediate energy range of 0.05 to 5.0 MeV, Compton scattering (CS) predominates, leading to a slight decrease in μ/ρ values.

The glass sample labeled M3, which contains 3% Nd, exhibits the highest μ/ρ values. This is attributed to neodymium's higher atomic number compared to other elements, which increases the μ/ρ values in the glass sample.

The HVL values for the produced glass samples were calculated using the estimated μ values and are illustrated in Fig. 6 as a function of photon energy. As shown in Fig. 6, HVL values increase with higher photon energy and decrease with greater Nd_2O_3 concentration. This behavior aligns with the earlier explanation of μm as a function of energy. According to the definition, materials with lower HVL values provide better shielding performance. The M3 glass sample used in the experiment exhibited the lowest HVL values, ranging from 0.00403 cm at 0.015 MeV to 6.0281 cm at 15 MeV.

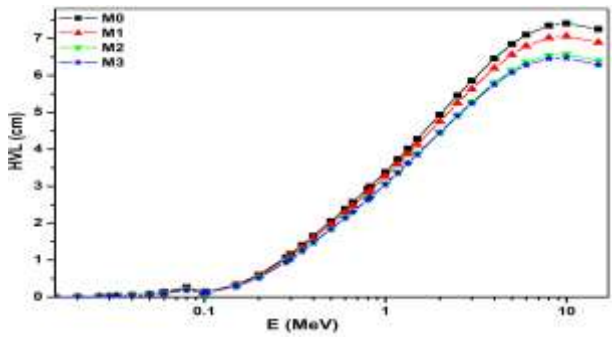

Fig. 6: HVL values for the prepared glasses as a function of the photon energy.

Additionally, the variations in Zeff and Nel for the produced glass samples across the photon energy range of 0.015–15 MeV are illustrated in Fig. 7a and 7b, respectively. These figures reveal that the changes in Zeff and Nel values for all samples follow a consistent trend.

Specifically, both Zeff and Nel significantly decrease as photon energy increases up to 0.08 MeV, despite a peak at 98 keV related to the K-absorption edge for Bi, where the photoelectric effect (PE) is predominant. Following this, from 0.1 to 1.5 MeV, all samples exhibit a slight reduction or fluctuation in Zeff and Nel values, reaching their lowest points at 1.6 MeV due to the influence of the Compton scattering (CS) process. In the 2–15 MeV range, both values steadily increase, indicating that the presence of neodymium enhances gamma-ray interactions, thereby reducing the number of photons that can penetrate the glass.

Among all the samples, M3 exhibits the highest Zeff and Nel values, ranging from 13.062 and 2.949 x 10^{23} at 1.5 MeV to 59.11 and 13.345 x 10^{23} at 20 keV, respectively. Generally, materials with higher Zeff provide better shielding against gamma rays, suggesting that M3 glass is a promising candidate for gamma radiation protection.

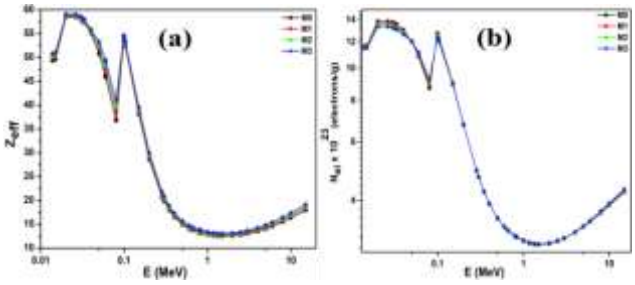

Fig. 7: Variation of (a) Zeff and (b) Nel for glass samples according to photon-energy.

6 Conclusions

Phosphate glasses doped with varying concentrations of Nd_2O_3, exhibiting densities between 3.13 g/cm³ and 3.49 g/cm³, were produced with high density. The VM values range from 60.84 cm³/mol to 50.5 cm³/mol, and the XRD pattern confirms the amorphous nature of the glass samples. The shielding properties improve with increasing Nd_2O_3 content. All glass samples exhibited high μ_m values, while the MFP, TVL, and HVL values were low. Particularly, the glass sample (M3) composed of (59% $NH_4H_2PO_4$ + 20% B_2O_3 + 5% ZnO + 10% Bi_2O_3 + 3% Na_2CO_3 + 3% Nd_2O_3) exhibited the lowest TVL, HVL, and MFP values, along with the highest μ_m value. The theoretical and experimental mass attenuation coefficients differ by less than 15%. The comparison of the best μ_m value (0.089 cm²/g) with that of lead (0.1101 cm²/g), shows that the former represents 81% of the lead value. The findings indicate that neodymium-doped phosphate glasses are effective gamma-ray shielding materials for various applications.

In summary, we demonstrate why Microsoft Word is useful, the font of the main text is 10 Times New Roman with single line spacing of 6 pt after and 0 pt before.

The titles are in font 12, bold and they have a single line spacing of 6pt before, and 12 pt after.

References

[1] El-Sharkawy, RM., Allam, EA., El-Taher, A., Elsaman, R., Massoud, EE., Mahmoud, ME., Synergistic effects on gamma-ray shielding by novel light-weight nanocomposite materials of bentonite containing nano Bi2O3 additive, Ceramics, **48 (5)**, 7291-7303,2022.

[2] M. Adib, N. Habib, I. Bashter, A. Saleh, Neutron transmission through pyrolytic graphite crystal II, Annals of Nuclear Energy,**38**, 802–807,2011.

[3] M. Adib, N. Habib, I. Bashter, M. Fathallah, A. Saleh, MgO single-crystal as an efficient thermal neutron filter Annals of Nuclear Energy, **38**,2673–2679, 2011.

[4] I. Akkurt, A. Calik, H. Akyıldırım, The boronizing effect on the radiation shielding and magnetization properties of AISI 316L austenitic stainless steel, Nucl. Eng. Des., **241 (1)**,55–58,2011.

[5] T. Kaur, J. Sharma, T. Singh, Feasibility of Pb-Zn binary alloys as gamma rays shielding materials, Int. J. Pure Appl. Phys. ,**13 (1)**,222–225, 2017.

[6] I. Akkurt, A. Calik, H. Akyıldırım, The boronizing effect on the radiation shielding and magnetization properties of AISI 316L austenitic stainless steel, Nucl. Eng. Des**., 241 (1)**,55–58, 2011.

[7] A. Saleh, Rizk Mostafa Shalaby, Nermin Ali Abdelhakim, comprehensive study on structure, mechanical and nuclear shielding properties of lead-free Sn–Zn–Bi alloys as a powerful radiation and neutron shielding material, Radiation Physics and Chemistry,**195**,110065, 2022.

[8] M. Adib, N. Habib, I. Bashter, H.N. Morcos, M. Fathallah, M.S. El-Mesiry, A. Saleh, Neutron characteristics of single-crystal magnesium fluoride, Annals of Nuclear Energy, **60**, 163–171,2013.

[9] Abdelmoneim Saleh, Hussain Almohiy, Rizk Mostafa Shalaby, Mohamed Saad, Comprehensive investigation on physical, structural, mechanical and nuclear shielding features against X/gamma-rays, neutron, proton and alpha particles of various binary alloys, Radiation Physics and Chemistry,**216**, 111443,2024.

[10] M. Dong, et al., A novel comprehensive utilization of vanadium slag: As gamma ray shielding material, J. Hazard. Mater., **318**,751–757, 2016.

[11] M. Ambika, N. Nagaiah, S. Suman, Role of bismuth oxide as a reinforcer on gamma shielding ability of unsaturated polyester based polymer composites, J. Appl. Polym. Sci., **134 (13)**, 2017.

[12] A. Saleh, R. Elshazly, H. Abd Elghany, The Impact of CdO on the Radiation Shielding Properties of Zinc-Sodium-Phosphate Glass Containing Barium. *Arab Journal of Nuclear Sciences and Applications*, ***0*(0)**, 1–11, 2021.

[13] Negm, HH., Allam, EA., Abdeltwab, E., Mostafa, M Mahmoud, ME and El-Taher, A., A new nanocomposite of copper oxide and magnetite intercalated into Attapulgite clay to enhance the radiation shielding. Radiation Physics and Chemistry 216, 111398. 2024.

[14] Abdelmoneim Saleh, M. G. El-Feky, M. S. Hafiz, N. A. Kawady, Experimental and theoretical investigation on physical, structure and protection features of TeO2-B2O3 glass doped with PbO in terms of gamma, neutron, proton and alpha particles, Radiation physics, and chemistry,**202**,110586,2022.

[15] Hani Negm, Hend Abd-Allah, Atta Y Abdel-Latief, MA Abdel-Rahim, Atef El-Taher, Nagih M Shaalan., Fabrication and characterization of structured Zn1-xCdxWO4 (0≤ x≤ 1) with tunable photoluminescent and promising applicable heterometallic nanocomposites in shielding properties. Radiation Physics and Chemistry 215, 111335. 2024.

[16] Abdelmoneim Saleh, Comparative shielding features for X/Gamma-rays, fast and thermal neutrons of some gadolinium silicoborate glasses, Progress in Nuclear Energy **154**, 104482,2022.

[17] A. Shahboub, G. El Damrawi, A. Saleh, A new focus on the role of iron oxide in enhancing the structure and shielding properties of Ag2O–P2O5 glasses, Eur. Phys. J. Plus., 136-947,2021.

[18] Mahmoud, ME., El-Sharkawy, RM., Allam, EA., Elsaman, R., El-Taher, A., Fabrication, and characterization of phosphor tungstic acid - Copper oxide nanoparticles - Plastic waste nanocomposites for enhanced radiation-shielding. J Alloys Compd., **803**,768-777 2019.

[19] Allam, EA., El-Sharkawy, RM., El-Taher, A., Shaaban, ER., Massoud, EE., Mahmoud, ME., Enhancement and optimization of gamma radiation shielding by doped nano HgO into nanoscale bentonite. Nuclear Engineering and Technology **54(6)**, 2253-2261, 2022.

[20] El-Sharkawy, RM., Allam, EA., El-Taher, A., Shaaban, ER and Mahmoud, ME., Synergistic Effect of Nano-bentonite and Nano cadmium Oxide Doping Concentrations on Assembly, Characterization and Enhanced Gamma-Rays Shielding Properties of Polypropylene Ternary Nanocomposites. International Journal of Energy Research,**45 (6)**, 8942-8959, 2021.

[21] Allam, EA., El-Sharkawy, RM., Shaaban, Kh. S., El-Taher, A., Mahmoud, ME., El Sayed, Y., Structural and thermal properties of nickel oxide nanoparticles doped cadmium zinc borate glasses: preparation and characterization Digest Journal of Nanomaterials & Biostructures (DJNB) 17 (1). 2022.

[22] El-Taher, A., Mahmoud, H.M. H.M and Abbady, Adel G.E., Comparative Study of Attenuation and Scattering of Gamma –Ray through Two Intermediate Rocks. Indian Journal of Pure & Applied Physics, 45 .2007

[23] Amer, t. E., El-hazel, M. N., Abdel Fattah, N.A, El-shamy, A.S., Abdellah, W. M. and El-shahat, M .F. Processing of Abu Zeneima mineralized gibbsite ore material for the recovery of aluminum, zinc, and individual light rare earth oxides. Isotope and Radiation Research Journal,**41(4s1)**, 1163-1177, 2009.

[24] Meshari Almeshari, Fawzy Hammad Sallam, Mohamed Tharwat, Yasser Alzamil, Mohammed Salih, Bader Alshoumr, Amjad Alyahyawi, Atef El-Taher., Preparation and structure investigation of polyethylene terephthalate polyester reinforced Ni0. 5Zn0. 5Fe2O4 nanoparticles for gamma ray shielding performance. Physica Scripta 99 (5), 055311. 2024.

[25] Kaur S, Singh GP, Kaur P, Singh DP, Cerium luminescence in borate glass and effect of aluminum on blue-green emission of cerium ions. J Lumin., **143** ,31–37 ,2013.

[26] El-Fiki, S., El Kameesy, S.U., Nashar, D.E.E., Abou-Leila, El-Mansy M.A., Ahmed, M., Influence of bismuth contents on mechanical and gamma-ray attenuation properties of silicone rubber composite, Int. J. Adv. Res. ,**3(6)**, 1035–1039, 2015.

[27] Gounhalli S.G., Shantappa A., Hanagodimath S.M., Studies on mass attenuation coefficient, effective atomic numbers and electron densities of some narcotic drugs in the energy range 1KeV–100GeV, IOSR J. Appl. Phys., (IOSR-JAP),**2(4),** 40–48, 2012.

[28] Berger M. J., Hubbell J.H., XCOM: Photon cross sections database, Web Version, 1.2. National Institute of Standards and Technology, Gaithersburg, MD20899, USA. (Originally published as NBSIR 87-3597 ‘‘XCOM: Photon Cross Sections on a Personal Computer’’).,1999.

[29] Saddeek, Y B., Shaaban, KH.S, Elsaman, R., El-Taher, A., Amer, T.Z., Attenuation-density anomalous relationship of lead alkali borosilicate Glasses. Radiation Physics and Chemistry,**150**,182–188, 2018.

[30] U Rilwan, GM Aliyu, SF Olukotun, MM Idris, AA Mundi, S Bello, I Umar, A El-Taher, KA Mahmoud., 2024 Recycling and characterization of bone incorporated with concrete for gamma-radiation shielding applications. Nuclear Engineering and Technology.56, 7, 2828-2834.

[31] Ali A.A., Rammah Y.S., Shaaban M.H., The influence of TiO_2 on structural, physical and optical properties of B_2O_3 –TeO_2 – Na_2O – CaO glasses, J. Non. Cryst. Solids, **514**, 52–59, 2019.

[32] Bagheri R., Moghaddam A.K., Yousefnia H., Gamma-ray shielding study of barium-bismuth-borosilicate glasses as transparent shielding materials using MCNP-4C Code, XCOM program, and available experimental data. Nucl. Eng. Technol. ,(49),216–223,2017.

[33] Saleh A., El-Feky M. G., Hafiz M. S., Kawady N. A., Experimental and theoretical investigation on physical, structure and protection features of TeO2-B2O3 glass doped with PbO in terms of gamma, neutron, proton, and alpha particles, Journal of Radiation Physics and Chemistry,202,110586,2023.

[34] Gerard, L., Guilbert, N., Jensen, K.B., Levring, H.,

WinXCom - a program for calculating X-ray attenuation coefficients., Radiat. Phys. Chem.,**04.**040,2004.

[35] A. Mardhiah, W. Hanif, K. Azman, N. Yahya, The Physical Properties Of Lead Borate (PbO-B2O3)Glass. KONAKA,2015.

[36] Borsella E, Vecchio AD, Garca MA, Sada C, Gonella F, Polloni R, et al. Copperdoping of silicate glasses by the ion-exchange technique: a photoluminescence spectroscopy study. J Appl Phys.,2002.

[37] Idris M.M., Ewa M. K., Iwa S. J., Isah S. H., and Suleiman A., Investigation Of (Pb2O3)x(SnO2)1-x Photon Shielding Capabilities For Medical Radiation Application. J. Rad. Nucl. Appl., **8**, 209-213,2023.

[38] El-Fiki S., El Kameesy S., Nasha D. r, Abou- Leila, El-Mansy M.A., Ahmed M., Influence of bismuth contents on mechanical and gamma-ray attenuation properties of silicone rubber composite, International Journal of Advanced Research. h, **(3)**, 1035–1039,2015.

[39] Bagheri R., Shirmardi S., Ruhollah A., Study on Gamma-ray Shielding Characteristics of Lead Oxide, Barite, and Boron Ores using MCNP-4C Monte Carlo code and Experimental data, Journal of Testing and Evaluation., **45**, 2259-2266,2016.

[40] Un A., Sahin Y., Determination of mass attenuation coefficients, effective atomic and electron numbers, mean free paths and kermas for PbO, barite, and some boron ores, journal of Nuclear Instruments and Methods in Physics Research Section B: Beam Interactions with Materials and Atoms., **269**, 1506-1511,2011,

[41] Bagheri R., Shirmardi S., Ruhollah A. Study on Gamma-ray Shielding Characteristics of Lead Oxide, Barite, and Boron Ores using MCNP-4C Monte Carlo code and Experimental data, Journal of Testing and Evaluation., **45**, 2259-2266,2016.

[42] Ahmed Khalil, Ibrahim I Bondouk, Elhassan A Allam, Islam M Nabil, Mogahed Al-Abyad, Heba Saudi, Atef El-Taher, Mohamed E Mahmoud, Ahmed Amar., A binary composite material of nano polyaniline intercalated with nano-Fe2O3 for enhancing gamma-radiation-shielding properties: experimental and simulation study. Progress in Nuclear Energy 169, 105067. 2024

[43] El-Taher, A., Hesham MH Zakaly, Rehab El-Sharkawy, Elhassan A Allam, Meshari Al Meshari, Mohamed E Mahmoud., Effect of bismuth oxide nanoparticles on the radiation shielding of bentonite clay using Fluka modeling calculations and simulation studying. Progress in Nuclear Energy 155, 10449. 2023.

[44] El-Taher, A., Ali, AM., Saddeek, YB., Elsaman, R., Algarni, H., Shaaban, KS., Amer, T.Z., Gamma-ray shielding and structural properties of iron alkali alumino-phosphate glasses modified by PbO. Radiation Physics and Chemistry, **165**, 108403, 2019.

[45] El-Taher, A., Zakaly, HMH., Pyshkina, Mariia., Allam, EA., El-Sharkawy, RM., Mahmoud, ME., Mohamed AE Abdel-Rahman., A comparative Study Between Fluka and Microshield Modeling Calculations to study the Radiation-Shielding of Nanoparticles and Plastic Waste Composites. Zeitschrift für anorganische und allgemeine Chemie .,**647 (10),** 1083-1090,2021.

[46] Deol S., Pardeep Kaur, Singh J., Kaur P., Vermani Y., Singh T., Gamma-Ray Sensing Properties of Nd Doped Phosphate Glasses, Journal of Physics: Conference Series, **2426**,012034,2023.

Dissertations and Theses

Author: *M.S.Hafiz*. Assistant lecturer M.A. thesis, University of Menoufeia , Eygpt, 2021.